UNIVERSITY OF AMSTERDAM

UvA-DARE (Digital Academic Repository)

Understanding and tuning sliding friction

Liefferink, R.W.

Publication date
2021

Link to publication

Citation for published version (APA):
Liefferink, R. W. (2021). *Understanding and tuning sliding friction*. [Thesis, fully internal, Universiteit van Amsterdam].

General rights
It is not permitted to download or to forward/distribute the text or part of it without the consent of the author(s) and/or copyright holder(s), other than for strictly personal, individual use, unless the work is under an open content license (like Creative Commons).

Disclaimer/Complaints regulations
If you believe that digital publication of certain material infringes any of your rights or (privacy) interests, please let the Library know, stating your reasons. In case of a legitimate complaint, the Library will make the material inaccessible and/or remove it from the website. Please Ask the Library: https://uba.uva.nl/en/contact, or a letter to: Library of the University of Amsterdam, Secretariat, Singel 425, 1012 WP Amsterdam, The Netherlands. You will be contacted as soon as possible.

UvA-DARE is a service provided by the library of the University of Amsterdam (https://dare.uva.nl)

Download date:24 May 2024

APPENDIX A

Sliding friction on ice

A.1 The penetration hardness of ice

The penetration hardness P_h is quantified with an indentation experiment where a sphere with a radius of $R = 1.6$ mm is pushed into the ice surface, see Section 2.2 for more details. For an indentation velocity v_ind of 3.8 μm/s the indentation depth δ as a function of the loading force N is plotted in Figure A.1 for several temperatures.

The measured penetration hardness, see Figure 5.2, is fitted with a polynomial regression on the variables temperature T (in °C) and the logarithm of the indentation speed $\ln(v_\mathrm{ind})$ with, respectively, 1 and 3 degrees:

$$\begin{aligned} P_\mathrm{h}(T, v_\mathrm{ind}) = {} & P_{00} + P_{10}T + P_{01}\ln(v_\mathrm{ind}) \\ & + P_{11}\,T\ln(v_\mathrm{ind}) + P_{02}\ln(v_\mathrm{ind})^2 \\ & + P_{12}\,T\ln(v_\mathrm{ind})^2 + P_{03}\ln(v_\mathrm{ind})^3\,. \end{aligned} \tag{A.1}$$

The fit parameters found, with a resulting coefficient of determination of $R^2 = 0.8885$, are $P_{00} = 8.041 \times 10^8$, $P_{10} = -3.337 \times 10^6$, $P_{01} = 1.465 \times 10^8$, $P_{11} = -2.645 \times 10^5$, $P_{02} = 8.936 \times 10^6$, $P_{12} = -6.282 \times 10^3$, and $P_{03} = 1.792 \times 10^5$. For a constant indentation speed of $v_\mathrm{ind} = 3.8$ μm/s, as used in Figures 5.2 and A.1, this fit results in a penetration hardness that linearly decreases with temperature as $P_\mathrm{h} = (-1.01\,T + 19.2) \times 10^6$.

Close to the melting point, pressure melting occurs; the melting temperature of ice decreases with increasing pressure because the liquid-phase density is lower than the solid phase. The pressure that has to be exceeded to melt ice is described by the Clausius-Clapeyron equation [175]:

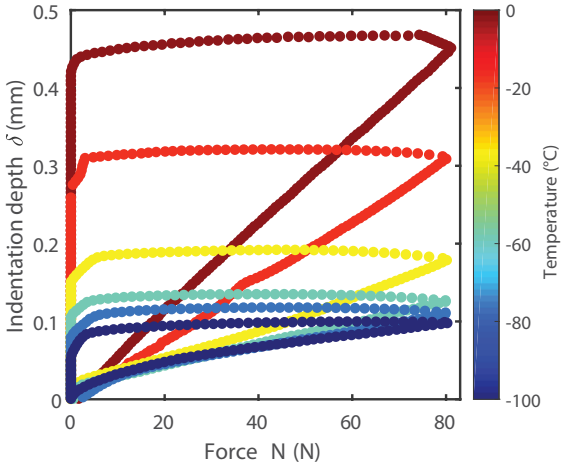

Figure A.1: Indentation depth δ as a function of the force N for an indentation speed of 3.8 μm/s captured with a hardness test for various temperatures.

$$P_{\mathrm{m}} = \frac{L}{T_0 \Delta V} T = -13.5 \times 10^6 \, T \,, \tag{A.2}$$

with $L = 3.34 \times 10^5$ J/kg the latent heat of fusion, $T_0 = 0$ °C the freezing point of water at a pressure of 1 bar, and $\Delta V = -9.05 \times 10^{-5}$ m^3/kg the change in specific volume from solid to liquid. For temperatures higher than -1.5 °C, the pressure necessary for pressure melting is lower than the penetration hardness. Therefore, the limiting pressure for -1.5 °C up to 0 °C in Figure 5.2 is described by the Clausius-Clapeyron equation.

A.2 Ploughing model

A spherical slider ploughing through ice, similar as ploughing through granular materials as described in Chapter 3, occurs when the contact pressure exceed the penetration hardness. In this plastic regime, the sphere indents into ice up to the contact area A_{c} can support the normal force: $A_{\mathrm{c}} = \frac{N}{P_{\mathrm{h}}(T)}$. This contact area, the projected area of contact in the normal direction, which is in contact with the ice surface, is $A_{\mathrm{c}} = \frac{1}{2}\pi r^2$, with r the radius of the ploughing track. The final depth of

indentation δ can be written, with the use of $\delta \approx \frac{r^2}{2R}$ for $\delta << R$, as $\delta = \frac{N}{\pi R P_\mathrm{h}(T)}$. Consequently, this indentation results in scratching ice with a ploughing area A_P and a ploughing force $F_\mathrm{P} = A_\mathrm{P} P_\mathrm{h}(T)$. The ploughing area is the cross-sectional area $A_\mathrm{P} \approx \frac{4}{3} r\delta$, and it can be rewritten as

$$A_\mathrm{P} = \frac{4\sqrt{2}}{3\pi^{3/2}R} \frac{N^{3/2}}{P_\mathrm{h}(T)^{3/2}} , \tag{A.3}$$

which results in a ploughing force of

$$F_\mathrm{P} = A_\mathrm{P} P_\mathrm{h}(T) = \frac{4\sqrt{2}}{3\pi^{3/2}R} \frac{N^{3/2}}{\sqrt{P_\mathrm{h}(T)}} . \tag{A.4}$$

With $\mu_\mathrm{P} = F_\mathrm{P}/N$, we get Equation (5.2).

Velocity-dependent ploughing model

To take into account the velocity dependency of the penetration hardness, as is shown in the inset of Figure 5.2(a) and fitted with Equation (A.1), the ploughing model has to be modified. Two velocities, and therefore two penetration hardnesses, are involved in ploughing: the indentation speed v_ind in the normal direction, where the ice is indented by the slider; and the sliding speed v_s in the tangential direction, the speed at which the final ploughing occurs. As the ploughing area A_P is set by the indentation in the normal direction, the corresponding penetration hardness is at the indentation speed:

$$A_\mathrm{P} = \frac{4\sqrt{2}}{3\pi^{3/2}R} \frac{N^{3/2}}{P_\mathrm{h}(T, v_\mathrm{ind})^{3/2}} . \tag{A.5}$$

The subsequent ploughing force is then based on the penetration hardness at the sliding speed and the calculated ploughing area A_P:

$$F_\mathrm{P} = \frac{4\sqrt{2}}{3\pi^{3/2}R} \frac{P_\mathrm{h}(T, v_\mathrm{s})}{P_\mathrm{h}(T, v_\mathrm{ind})^{3/2}} N^{3/2} . \tag{A.6}$$

Based on the sphere-on-ice geometry, we can calculate the indentation speed corresponding to the sliding speed and subsequently calculate the related penetration hardness for the ploughing force. The ratio of the related speeds is:

$$\frac{v_\mathrm{ind}}{v_\mathrm{s}} = \frac{\delta}{r} = \sqrt{\frac{N}{2\pi R^2 P_\mathrm{h}(T, v_\mathrm{ind})}} . \tag{A.7}$$

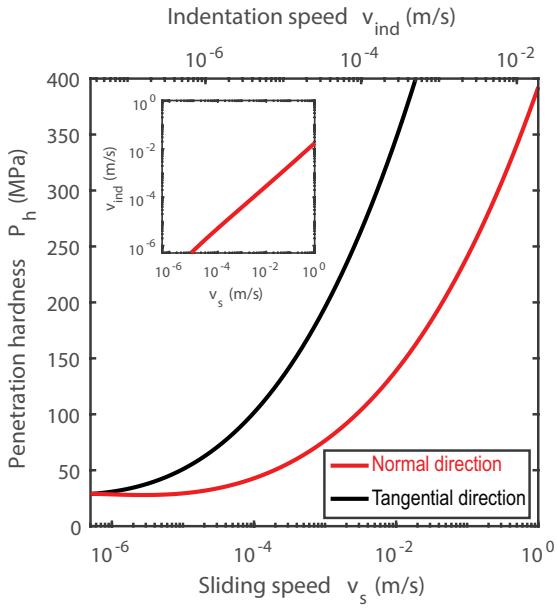

Figure A.2: Penetration hardness in the normal direction (red) and tangential direction (black) as a function of sliding speed for ice at a temperature of -20 °C based on Eq. (A.1). The calculated indentation speed corresponding to the set sliding speed is given in the inset and as top axes for sliding a glass sphere ($R = 1.84$ mm) at a normal force of 2.5 N over ice at -20 °C, Eq. (A.7). The indentation speed is around 4% of the sliding speed, and consequently, the penetration hardness in the normal direction is smaller than the penetration hardness in the tangential direction.

This nonlinear equation can be numerically solved to yield an indentation speed v_{ind} for a given sliding speed v_{s}. For a glass sphere sliding over ice at -20 °C, the resulting indentation speed as a function of the sliding speed is given in the inset of Figure A.2; the indentation speed is, in general, a fraction of the sliding speed, around 4%. Consequently, for a given sliding speed, we can calculate the penetration hardness in the normal and tangential directions; see Figure A.2. Finally, the friction force and friction coefficient can be calculated based on Equation (A.6), where the indentation speed is based on numerically solving Equation (A.7).

A.3 Contact mechanics

Soda-lime glass

To quantify the real contact area (RCA) and the average contact pressure P_c of the spherical sliders on ice, we use the Tribology Simulator (from Tribonet [62]). Based on the surface topography of the slider and the mechanical properties of the slider and the ice surface, the simulator solves the elastoplastic contact equations through a numerical boundary element model. The plastic limit is set by the penetration hardness of the ice in the normal direction, calculated for the set sliding speed $v_s = 0.38$ mm/s and temperature T, with the use of Equations (A.1) and (A.7).

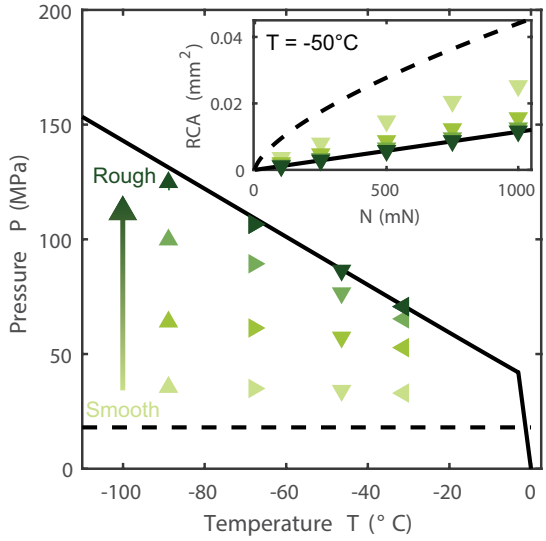

Figure A.3: Pressure P as function of the temperature T for glass spheres with surface roughnesses 98, 222, 575, and 3077 nm at a normal force of 500 mN. The smoothest sphere is mainly elastic where, for increasing surface roughnesses, the pressure increases until the plastic limit is reached. The dashed and solid lines are, respectively, the elastic Hertzian pressure and the penetration hardness P_h of the ice. For the latter, the penetration hardness in the normal direction for the set sliding speed of 0.38 mm/s is used. Inset: RCA as a function of the normal force N. Indenpendent of the surface roughness, the real contact area increases linearly with the normal force. Therefore, the contact pressure is almost independent of the normal force.

In Figure A.3, the contact pressure as a function of temperature is given for glass spheres with surface roughness S_q from 98 nm to 3077 nm. The dashed and solid lines represent, respectively, the elastic Hertzian contact pressure [176] and the plastic limit given by the penetration hardness as N/P_h. For increasing surface roughnesses, the contact mechanics convert from a mainly elastic contact to a plastic contact. The RCA increases linearly, even for the relatively smooth sphere, with the normal force, as is given in the inset of Figure A.3. Therefore, the contact pressure is almost independent of the normal force.

Silicon carbide

In Figure A.4, the real contact area for the SiC spheres is given as a function of the normal force. Both spheres, with radii of 6.00 (red) and 0.75 mm (blue), have a mainly elastic contact with the ice surface at −50 °C (open circles) and at −90 °C (closed circles). The large sphere has a large RCA and, due to the finite size of the measured surface topography (208 by 208 μm), can only be calculated up to 400 mN.

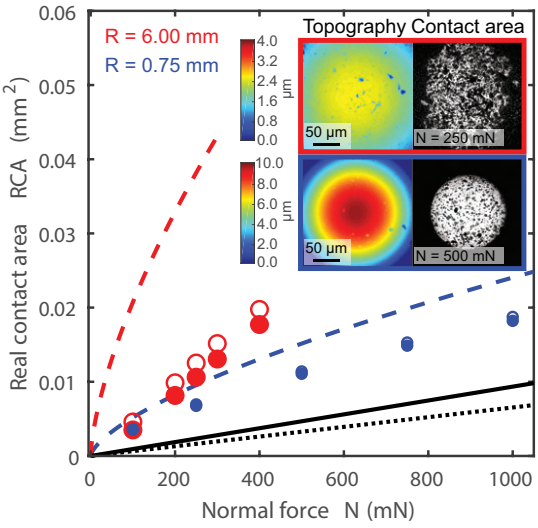

Figure A.4: Contact mechanics of the SiC spheres sliding on ice and RCA as a function of normal force N for a sphere with a radius of 6.00 mm (red) and 0.75 mm (blue) at temperatures of −50 °C (open circles) and −90 °C (closed circles). The dashed lines represent the elastic Hertzian pressure. The solid and dotted lines are, respectively, the plastic limit set by the penetration hardness at temperatures of −50 °C and −90 °C. Inset: surface topography (left) and calculated area of real contact (right) for the SiC spheres.

Sapphire

The contact mechanics for a sapphire sphere on ice are given in Figure A.5. The contact is mainly elastic due to the low surface roughness (28 nm). Therefore, the RCA increases, as expected for an elastic Hertzian contact [176], sublinearly with the normal force. The RCA for a normal force of 500 mN is used to quantify the shear stress and contact pressure.

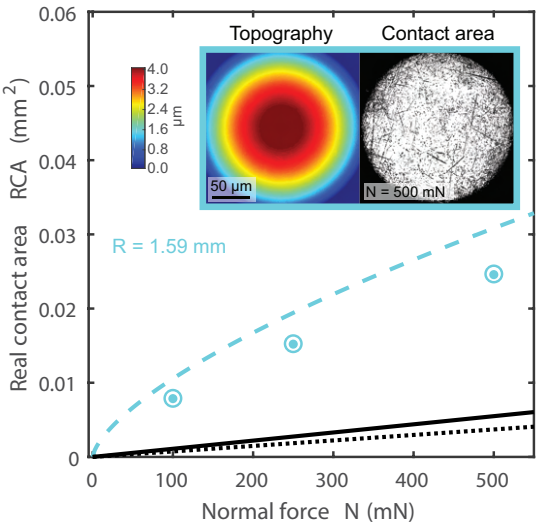

Figure A.5: Contact mechanics of a sapphire sphere (radius of 1.59 mm) sliding on ice and RCA as a function of the normal force N at temperatures of -50 °C (open circles) and -90 °C (closed circles). The dashed line represents the elastic Hertzian pressure and the solid and dotted lines are, respectively, the plastic limit set by the penetration hardness at temperatures of -50 °C and -90 °C. Inset: surface topography (left) and calculated area of real contact (right) for the sapphire sphere.

A.4 Ploughing on the microroughness scale

Ploughing not only occurs on the macroscale of the slider-on-ice contact; single asperities can plastically deform the ice and therefore plough through it tangentially. In Figure 5.3(b), the ploughing tracks that were left on the ice after a sphere slid over the ice surface are given. For a high surface roughness, $S_q = 3077$ nm, the measured ploughing area ($A_P = 7.8 \times 10^{-11}\ m^2$) results in a friction coefficient based on ploughing of $\mu_P = 0.07$ [for $N = 0.21$ N, penetration hardness in the normal direction $P_h = 194$ MPa and using Equation (5.2)]. As the increase in the friction coefficient for the highest surface roughness relative to the lowest surface roughness is $\Delta\mu = 0.24$, the ploughing can only explain 30% of the increased friction. Based on the measured surface topography, a ploughing area of ($A_P = 12.2 \times 10^{-11}\ m^2$)

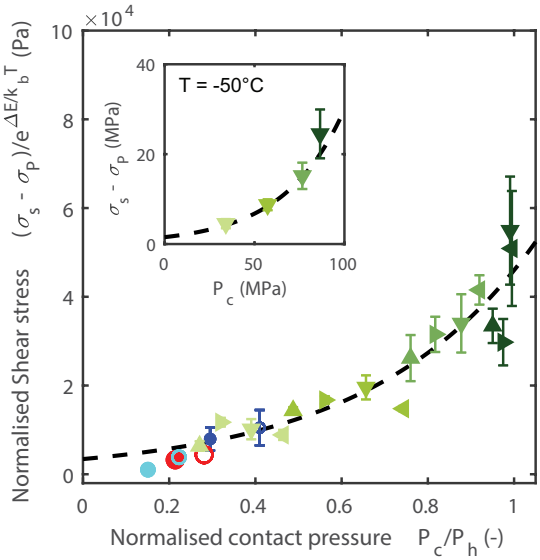

Figure A.6: Normalised effective shear stress $(\sigma_s - \sigma_P)/e^{\Delta E/k_B T}$ as a function of the normalised contact pressure P_c/P_h for various sliders, surface roughnesses, and temperatures at a sliding speed of 0.38 mm/s. Here, the effective shear stress is based on the measured friction force, excluding the ploughing contribution. The ploughing can explain up to 40% of the observed increased friction. The dashed line is a fit using Eq. (5.4). The same symbols and colours are used as in Fig. 5.4. Inset: effective shear stress $\sigma_s - \sigma_P$ as a function of the contact pressure P_c for various glass sliders with increasing surface roughness at $T = -50$ °C and a sliding speed of 0.38 mm/s.

can be calculated [see gray area in the top panel of Fig. 5.3(b)]. As the orientation of the sphere on ice is not the same, a small difference is found compared with the measurements in both the ploughing track and the ploughing area. Now, the ploughing can explain 40% of the observed increased friction.

In Figure A.6, the increase of shear stress with increasing contact pressure where the ploughing is excluded is given. For the ploughing stress $\sigma_P = F_P/\mathrm{RCA}$, a ploughing force based on the quantified plastic indentation of the surface topography is used. We can model the effective shear stress $\sigma_s - \sigma_P$ as Equation (5.4) with $\sigma_0 = 3.4$ kPa and $b = 2.6$. Consequently, if ploughing is taken into account, the shear stress set by the mobility of the ice surface is, although smaller, still the main contribution to the friction force.